foods

MDPI

Article

SC2-3, a Marine Nutrient Glycopeptide from *Nereis succinea*: Alleviating Cyclophosphamide-Induced Immunocompromise in Mice via M1-Type Macrophage Polarization

Yulin Liu [1,†], Yanan Huang [1,†], Jiaqi Li [1], Yiping Zhang [2] and Peipei Wang [1,3,4,*]

[1] College of Food Science and Technology, Shanghai Ocean University, Shanghai 201306, China; ylliu0807@163.com (Y.L.); 18638611062@163.com (Y.H.); i18032301787@outlook.com (J.L.)
[2] Technical Innovation Center for Utilization of Marine Biological Resources, Third Institute of Oceanography, Ministry of Natural Resources, Xiamen 361005, China; ypzhang@tio.org.cn
[3] National Experimental Teaching Demonstration Centre for Food Science and Engineering, Shanghai Ocean University, Shanghai 201306, China
[4] Marine Biomedical Science and Technology Innovation Platform of Lin-Gang Special Area, Shanghai 201306, China
* Correspondence: ppwang@shou.edu.cn; Tel.: +86-136-8170-5312
† These authors contributed equally to this work.

Abstract

Immunodeficiency is a global health concern, partly due to disrupted rhythms and drugs. Marine glycopeptides, with immunomodulatory and intestinal barrier protective activities, show great potential in dietary supplements and functional foods. Here, a marine glycopeptide, SC2-3, with a molecular weight of 5061 Da, was isolated and purified from *Nereis succinea*. Monosaccharide composition, NMR data, amino acid composition analysis, and SDS-PAGE analyses identified SC2-3 as a glycopeptide. The N-glycome results of SC2-3 collected by MALDI-TOF-MS revealed that SC2-3 contains fucosylated N-glycans with shorter glycan chains compared to human-derived N-glycans. SC2-3 exerted a significant immune-enhancing effect on macrophages in vitro. In vivo, in cyclophosphamide-induced immunocompromised mice, SC2-3 at different concentrations elevated organ indices, blood cell counts, and serum levels of IL-1β, TNF-α, and IL-6, while repairing cyclophosphamide-damaged/atrophied tissues. Mechanistically, SC2-3 induced the differentiation of RAW264.7 cells toward an M1-like activation profile, significantly promoting the release of NO and ROS, upregulating the secretion of pro-inflammatory cytokines (IL-1β, TNF-α, and IL-6), and activating the TLR4/NF-κB signaling pathway. Additionally, SC2-3 upregulated intestinal epithelial tight junction proteins and normalized the overexpression of MUC-2, thereby maintaining intestinal barrier integrity. These findings indicated the potential efficacy of the glycopeptide SC2-3 derived from natural marine sources in immunomodulation and protection of intestinal health.

Keywords: *Nereis succinea*; glycopeptide; structural characterization; immunoactivity; macrophage polarization

Check for updates

Academic Editor: Vincenzo Cunsolo

Received: 2 February 2026
Revised: 24 February 2026
Accepted: 1 March 2026
Published: 4 March 2026

Copyright: © 2026 by the authors. Licensee MDPI, Basel, Switzerland. This article is an open access article distributed under the terms and conditions of the Creative Commons Attribution (CC BY) license.

1. Introduction

Immune function is a fundamental defense mechanism that protects the body against exogenous pathogens and maintains internal homeostasis [1,2]. Immunodeficiency has become a public health issue of global concern. Multiple factors, including disrupted work–rest patterns, chronic psychological stress, and drug interventions, can directly impair

immune function, leading to a range of health problems such as tissue damage and reduced host resistance. These effects substantially diminish quality of life. In this context, the development of safe and effective strategies for immune regulation has become a critical need for alleviating immunosuppression and maintaining overall health. Immunomodulatory dietary supplements are a class of functional nutritional products designed with immune regulation as their core objective. Their mechanism of action does not involve non-specific activation of the immune system to amplify immune responses; rather, they deliver bioactive immune components to precisely modulate immune cell function, thereby optimizing the magnitude, duration, and specificity of the immune response and enhancing host defense against pathogens. As such, these supplements are distinct from interventions intended to "stimulate" the immune system. Their fundamental goal is to restore or maintain immune homeostasis—that is, to sustain the immune system in a dynamic state of equilibrium between appropriate responsiveness and self-tolerance through gentle and sustainable nutritional intervention [3]. Since the mid-20th century, immunomodulatory dietary supplements derived from natural raw materials have gradually gained public attention; however, the development of products with clearly defined efficacy targets and robust scientific validation has progressed relatively slowly [4,5]. Although certain products containing specific bioactive ingredients, such as Ganoderma lucidum extract, yeast β-glucan, and ginsenosides, have obtained GRAS (Generally Recognized as Safe) status from the U.S. FDA or have been registered as health foods in China, the overall development of immunomodulatory dietary supplements still faces significant bottlenecks. This limitation is reflected not only in the homogenization of product portfolios, but more fundamentally, in the relative lag of basic research [6,7].

When exploring substances with immunomodulatory functions, polysaccharides have attracted much attention due to their good safety and superior immunomodulatory properties [8–14]. It is noteworthy that certain marine glycopeptides have been shown to indirectly target key immune signaling pathways, such as TLR4, by regulating immune cell maturation and differentiation as well as cytokine secretion. In addition, marine-derived glycopeptides, originating from natural marine biological resources, generally exhibit favorable biocompatibility. This characteristic renders them promising candidates for application in immunomodulatory dietary supplements. Marine glycopeptides are a typical type of glycoconjugate, formed by the combination of polysaccharides and proteins or peptides from marine resources [15]. The structural diversity and novelty of marine-derived glycoconjugates are closely associated with the extreme environmental conditions, such as high pressure, low temperature, oligotrophy, and aphotic zones, in which their source organisms reside. At present, several studies have found that Marine glycopeptides possess biological activities such as immune regulation, antioxidation, anti-inflammation, antibacterial, and antiviral [15–19]. They can regulate immune responses through various pathways, for instance, promoting the proliferation and activation of immune cells, enhancing the secretion of cytokines, and improving the phagocytic function of macrophages [20,21]. This wealth of marine life, with its diverse and distinctive biological molecules, including the structurally unique glycopeptides, holds great promise for unlocking new possibilities in the development of immunomodulatory agents. However, partially due to the difficulty of glycopeptide extraction and purification techniques as well as structural analysis, there have been few extensive studies reported on marine glycopeptides so far.

Nereis succinea, a marine creature with high protein and low fat, has a long tradition of being used for food and medicine in East and Southeast Asia. Modern nutritional research shows that the ragworm is rich in various unsaturated fatty acids, such as ω-3, the eight amino acids essential for the human body, and multiple trace elements such as iron and zinc [22–24]. So far, the research and development of marine-derived bioactive glycopep-

tide dietary supplements have mainly focused on classic marine resources such as sea cucumbers and brown algae, and a more systematic research system has been established. In contrast, although *Nereis succinea*, as a high-protein, low-fat marine organism, has a long edible tradition in East Asia and has isolated anti-inflammatory and anticoagulant peptides from it [25–27], representing a marine biological resource with considerable development potential, the research on glycopeptide components is still in its infancy. Although preliminary evidence suggests that extracts from *Nereis succinea* possess certain immunoprotective effects [6,7], a critical scientific gap remains regarding its glycopeptide components that urgently requires investigation. This gap is primarily driven by the inherent structural complexity of *Nereis succinea* glycopeptides, including glycosylation sites and glycan chain composition, which substantially elevates the difficulty of structural characterization and thereby constrains in-depth investigations into their bioactive mechanisms and molecular targets. These existing uncertainties hinder the provision of effective theoretical guidance for optimizing extraction processes and developing *Nereis succinea* glycopeptides as functional dietary supplements. Therefore, further in-depth fundamental research and application-oriented exploration are urgently warranted.

In this study, a glycopeptide (named SC2-3) was extracted and purified from *Nereis succinea*. Its structural characteristics were preliminarily clarified, and its immunomodulatory activity and mechanism were evaluated in a cyclophosphamide (CTX)-induced immunosuppressive mouse model, with a focus on its ability to restore immune function and protect against chemical-induced damage. Collectively, SC2-3, a marine nutrient glycopeptide from *Nereis succinea*, could alleviate CTX-induced immunocompromise in mice via M1-Type macrophage polarization associated with the TLR4 signaling pathway.

2. Materials and Methods

2.1. Materials and Chemicals

Fresh *Nereis succinea* were obtained from Zhejiang, China, and identified by Prof. Shunsheng Chen, College of Food Science and Technology, Shanghai Ocean University. Monosaccharide standards, including L-rhamnose, L-fucose, L-arabinose, D-xylose, D-mannose, D-galactose, D-glucose, and galacturonic acid, were procured from Fluka Corporation (Buchs, Switzerland). Trifluoroacetic acid (TFA) and 1-phenyl-3-methyl-5-pyrazolone (PMP) were purchased from Sigma-Aldrich (Saint Louis, MO, USA). Cell Counting Kit-8 (CCK-8) was purchased from Adamas (Carson, NV, USA). The ROS and NO kits were obtained from Beyotime Biotechnology (Shanghai, China). DEAE-Cellulose column and Sephadex S-100 High Resolution resin were obtained from Cytiva Co., Ltd. (Uppsala, Sweden). All other reagents were of analytical grade.

2.2. Extraction and Separation of Glycopeptide

Fresh *Nereis succinea* tissue (1000 g, wet weight) was homogenized and subjected to defatting by stirring with acetone (1:1, w/v) at room temperature for 12 h. This procedure was repeated three times, followed by centrifugation at 8000 r/min (8228× g, r = 11.5 cm) for 20 min. The precipitate was air-dried overnight at room temperature to obtain defatted powder. The defatted powder was suspended in 0.1 M phosphate buffer (pH 6.0) at a concentration of 50 mg/mL. Enzymatic hydrolysis was performed by adding papain (Sigma-Aldrich, P4762, ≥10 U/mg) to a final concentration of 2.5% (w/v), and the mixture was incubated at 60 °C for 12 h. After cooling, the pH was adjusted to 8.0, and trypsin (Sigma-Aldrich, T1426, ≥10,000 U/mg) was added to a final concentration of 2.5% (w/v). The hydrolysis was continued at 37 °C for 12 h, followed by heating at 100 °C for 15 min to inactivate the enzymes. The supernatant was centrifuged, concentrated by rotary evaporation, dialyzed in deionized water (MWCO: 3500 Da, room temperature, water change every

4 h) for 3 days, and freeze-dried to obtain crude polysaccharide components. The crude extract was redissolved in water, added with 30% (*v*/*v*) trichloroacetic acid, and allowed to stand at 4 °C for 3 h to precipitate protein. The supernatant was collected by centrifugation, dialyzed for 3 days under the same conditions, concentrated and freeze-dried to obtain crude glycopeptide.

For the purification of the crude glycopeptide (SC), a DEAE-52 Cellulose column (Chromatographic column size: 600 mL Φ2.5 cm × 120 cm) was employed. Two-column volumes (1200 mL) were pre-balanced with deionized water at a flow rate of 6 mL/min. The crude SC was dissolved in 10 mL of deionized water, centrifuged at 10,000× *g* for 10 min, and the supernatant was taken. The sample volume was 10 mL (containing about 800 mg crude SC). The samples were eluted with deionized water step by step, followed by 0.2 M NaCl, 0.5 M NaCl, 1 M NaCl, and 2 M NaCl solution (each 600 mL) at a flow rate of 1 mL/min. Carbohydrates were detected using the phenol–sulfuric acid method, and the eluent was monitored by measuring the absorbance at 490 nm. The fractions (6 mL/tube) were collected. The components containing 0.2 M NaCl eluent were combined and concentrated, and the (MWCO: 3500 Da) was dialyzed with deionized water for 3 days and freeze-dried. For further purification, the 200 mg SC2 fraction was dissolved in 5 mL of deionized water and centrifuged. The supernatant was collected on a Sephadex S-100 high-resolution column (Φ2.5 cm × 120 cm, bed volume 600 mL) pre-equilibrated with 0.2 M NaCl (pH 7.0) for 2 column volumes (1200 mL). The same buffer was used for elution, and the flow rate was 0.3 mL/min. The eluent was detected using the phenol–sulfuric acid method at 490 nm for carbohydrates, and the flow fraction (6 mL/tube) was collected. The main peak (SC2-3) was combined, dialyzed, and freeze-dried.

The endotoxin content of the final product was determined using a Limulus Amebocyte Lysate (LAL) Endotoxin Assay Kit (Beyotime C0266BS, gel agglutination method). The measured endotoxin level of SC2-3 was 0.03 EU/mg (exact value based on triplicate measurements). To assess potential interference in cellular assays, we calculated the total endotoxin units added per well at the highest concentration used in macrophage experiments (1000 μg/mL). In a 96-well plate with a culture volume of 100 μL per well, the total endotoxin per well was (1000 μg/mL × 0.1 mL) × 0.03 EU/μg = 0.003 EU/well. This level is substantially below the threshold typically considered to induce non-specific macrophage activation (generally >0.1 EU/mL in culture medium, confirming that the observed immunostimulatory effects are attributable to SC2-3 itself rather than endotoxin contamination.

2.3. Structural Characterization

2.3.1. General Analysis

The total sugar content was determined using the phenol–sulfuric acid method. Glucose was used as the standard, the detection wavelength was 490 nm, and the linear range of the standard curve was 0.1–0.6 mg/mL. It should be noted that the total sugar determined by this method does not include uronic acid components. The content of uronic acid was determined using the sulfated borax–carbazole method. Galacturonic acid was used as the standard, the detection wavelength was 530 nm, and the linear range of the standard curve was 0–0.3 mg/mL. Protein content was measured using the Bicinchoninic Acid (BCA) protein assay kit [28,29]. According to our previous reports, the monosaccharide composition of SC2-3 was determined using the IC method. The relative molecular mass of SC2-3 was determined using high-performance gel permeation chromatography (HPGPC). The chromatographic system was equipped with a TSKgel G4000PWXL and a TSKgel G2500PWXL gel column (7.8 mm × 300 mm) in series, connected to a refractive index detector. The mobile phase was a 0.15 mol/L NaNO3 solution, the flow rate was 0.5 mL/min, and the column temperature was 35 °C. The molecular weight of SC2-3 was

calculated based on a calibration curve of log(Mw) versus retention time established using a series of dextran standards with known molecular weights (5~270 KDa) [30].

2.3.2. Amino Acid Composition Analysis

The marine glycopeptide SC2-3 (5 mg) was accurately weighed and dissolved in 6 mol/L hydrochloric acid. The resulting solution was transferred to a sealed hydrolysis vial and hydrolyzed at 110 °C ± 2 °C for a duration of 24 h. After cooling to room temperature, filter the hydrolyzed solution through a 0.22 μm membrane. Transfer the filtrate into a 25 mL volumetric flask and adjust the volume accordingly. The solution is then dried multiple times in a vacuum drying oven. Finally, dissolve the residue in sodium citrate buffer, mix thoroughly, filter again through a 0.22 μm membrane, and the ultra-high-speed automatic amino acid analyzer (Hitachi LA8080, Tokyo, Japan) was used for detection.

Methodological note: It should be noted that the standard acid hydrolysis method employed leads to the complete destruction of tryptophan (Trp); therefore, no data for this amino acid are included. Under acid hydrolysis conditions, asparagine and glutamine were deamidated to produce aspartic acid and glutamic acid, respectively. Therefore, the measured values of Asp and Glu in this paper were calculated as Asx and Glx. Additionally, sulfur-containing amino acids (e.g., Cys, Met) are susceptible to oxidation during the process, and their quantified values should be interpreted with caution.

2.3.3. SDS-PAGE

Marine glycopeptide SC2-3 was diluted using SDS-PAGE sample loading buffer (Beyotime, Shanghai, China), denatured, and loaded with 15% BeyoGel^{TM} SDS-PAGE precast gels (Beyotime, Shanghai, China). The sample volume was 30 μg protein and was electrophoresed according to the instructions of the kit. After the electrophoresis process, the gel was fixed with 75% ethanol for 30 min, oxidized with 1% periodate for 1 h, washed with water, soaked in 0.1% sodium sulfite for 20 min, stained with Schiff reagent for 1 h, washed with 0.1% sodium metasulfite overnight, and photographed. Then it stained with Coomassie brilliant blue (15 min) and photographed for analysis. (Methodological Notes: The reduction condition was 50 mM dithiothreitol (DTT) in the sample loading buffer. The heating denaturation conditions were 100 °C, 10 min; the protein quantification method is the BCA method).

2.3.4. NMR

For NMR analysis, SC2-3 was dehydrated, exchanged, and dissolved in 0.5 mL D_2O under vacuum. Using acetone as the internal standard (^{1}H δ 2.05, ^{13}C δ 31.05), ^{1}H-NMR and ^{13}C-NMR spectra were recorded using a Bruker AVANCE 500 MHz spectrometer (Billerica, MA, USA). The sample concentration was 10 mg/mL, and the temperature was 298 K; 1 H-NMR (64 scans, relaxation delay 2.0 s, pulse angle 45°), 13 C-NMR (20,000 scans, relaxation delay 2.0 s, pulse angle 30°, power-gated decoupling); the spectra were corrected by baseline/phase correction and calibrated in acetone.

2.3.5. N-Glycome

The glycopeptide was reduced with DTT (DTT: protein (1:1 w/w)) and alkylated with IAA (IAA: protein (2.5:1 w/w)). Then the supernatant was dialyzed against 10 mM ammonium bicarbonate (PH 8.6) for 48 h and lyophilized. The lyophilized glycopeptide was incubated with trypsin (100 μg protein, 50 mM NH3 HCO3 3 pH 8.0, 2 μg enzyme, 37 °C 16 h, 100 °C 5 min inactivated.) overnight and digested with peptide N-glycosidase F (P0708S, New England Biolabs, Hitchin, UK, 2 μL/2000 units, 1 × GlycoBuffer 2 pH 7.5, 37 °C) for 12 h to release the N-glycans. The released N-glycans were purified through

graphite cartridges (57088, Sigma, St. Louis, MO, USA) and eluted with 50% (*v*/*v*) acetonitrile containing 0.1% (*v*/*v*) TFA. Then the collected eluent was lyophilized. The N-glycans were permethylated using sodium hydroxide and iodomethane in DMSO and then analyzed using a MALDI-TOF mass spectrometer in positive mode (Positive ion reflection mode, DHB matrix 20 mg/mL in 70% ACN/0.1% TFA, loading volume of 1 μL about 5–10 μg original glycopeptide, mass range m/z 1000–5000, cumulative 500 laser shooting, external standard calibration). Glycan compositions were determined by database searching using GlycoWorkbench software v.2.1.4. It should be noted that the cleavage efficiency of PNGase F can be influenced by variations in the core structure of N-glycans. The N-glycomic profiling of SC2-3 is predicated on the assumption of complete N-glycan release by peptide N-glycosidase F. Accordingly, the N-glycan candidates identified via database matching are preliminary in nature, and their confidence levels are dependent on the matching scores and the quality of the reference database.

2.4. In Vitro Immune Activity of SC2-3

2.4.1. Cell Culture

Mouse mononuclear macrophages (RAW264.7) were purchased from Servicbio (Wuhan, China), and the cells were cultured in DMEM medium (Gibco, Brooklyn, NY, USA) containing 10% serum (Gibco, USA) and 1% penicillin–streptomycin solution (Absin, Shanghai, China) at 37 °C with 5% CO_2. All experiments in this study were performed using cells within a passage range of 8 to 12.

2.4.2. Evaluation of Cell Viability

RAW264.7 cells were seeded evenly in 96-well cell culture plates (density: 1×10^4/well) and allowed to adhere. After cell attachment, cells were treated with various concentrations of marine glycopeptide SC2-3 (25, 50, 100, 200, 400, 800, and 1000 μg/mL) for 48 h. Subsequently, the culture supernatant was removed, and a medium containing 10% CCK-8 reagent (Adamas, Shanghai, China) was added. After incubation, absorbance was measured at 450 nm using a microplate reader. Each treatment was performed in six replicates, and all experiments were independently repeated three times. The average absorbance of cell-free background control wells was subtracted for data correction.

2.4.3. Phagocytosis Analysis

RAW264.7 cells were seeded evenly in 96-well cell culture plates (density: 1×10^4/well), and after 24 h of cell attachment, they were treated with different concentrations of SC2-3 and LPS (1 μg/mL), respectively. After the treatment, the supernatant was discarded, 0.1% neutral red solution was added, incubated at 37 °C for 1 h, and washed three times with PBS buffer. Then, 100 μL of cell lysate (ethanol/acetic acid, 1:1, *v*/*v*) was added to each well, and the absorbance was measured at 540 nm after standing at room temperature for 2 h. All experiments were performed in triplicate independently (three biological replicates), with each biological replicate consisting of three technical replicates.

2.4.4. Determination of NO (Nitrite) in Culture Supernatant

RAW264.7 cells were seeded evenly in 96-well cell culture plates (density: 1×10^4/well). After attachment, the culture medium was removed, and the cells were treated with various concentrations of SC2-3 in the presence or absence of lipopolysaccharide (LPS, 1 μg/mL). Following incubation, nitric oxide (NO) production in the culture supernatant was quantified using a commercial NO assay kit, according to the manufacturer's instructions. The standard curve of 0–100 μM sodium nitrite ($R^2 > 0.995$) was established synchronously in each detection to ensure the quantitative accuracy. The standard curve of 0–100 μM

sodium nitrite was established synchronously ($R^2 > 0.995$), and the interference of phenol red/serum was controlled.

To exclude the possibility that the observed immunostimulatory effects of SC2-3 were mediated by residual endotoxin contamination rather than the glycopeptide itself, a polymyxin B neutralization assay was performed in parallel. RAW264.7 cells were treated with SC2-3 (800 μg/mL) in the presence or absence of polymyxin B (10 μg/mL), a specific inhibitor of LPS-induced endotoxin activity. LPS (1 μg/mL) with or without polymyxin B was used as a control to verify the neutralizing efficacy. After 48 h of incubation, NO levels were measured as described above. A standard curve of 0–100 μM sodium nitrite ($R^2 > 0.995$) was established synchronously in each detection to ensure quantitative accuracy. All experiments were performed in triplicate independently (three biological replicates), with each biological replicate consisting of three technical replicates.

2.4.5. Intracellular Reactive Oxygen Species (ROS) Determination

The RAW264.7 cells were evenly spread on the cell culture plate, after 24 h of 96-well cell attachment (density: 1×10^4/well), and treated with different concentrations of SC2-3 for 48 h. The culture medium of 10 μmol/L DCFH-DA was added and incubated for 30 min, followed by washing the excess probe with serum-free medium, adding PBS, and then photographing and observing under a fluorescence microscope. The excitation wavelength was 488 nm, and the emission wavelength was 525 nm. Quantitative analysis was performed using ImageJ software 1.54g to measure the average fluorescence density. All experiments were performed in triplicate independently (three biological replicates), with each biological replicate consisting of three technical replicates.

2.4.6. Measurement of TNF-α, IL-1β, and IL-6

Mouse interleukin (IL-6), interleukin (IL-1β), and tumor necrosis factor (TNF-α) kits (Jingmei, Jiangsu, China) were used to measure the secretion levels of IL-1β, IL-6, and TNF-α in the cells. All experiments were performed in triplicate independently (three biological replicates), with each biological replicate consisting of three technical replicates.

2.4.7. MI Polarization of RAW264.7 Cells

RAW264.7 cells were inoculated in 6-well plates (density: 4×10^5/well), wall-approximated, and given treatment with 1 μg/mL LPS (Abmole, Houston, TX, USA), IL-4 (10 ng/mL), and different concentrations of SC2-3. After treatment, cells were washed and centrifuged to remove impurities. Fluorescently labeled antibodies (CD86-FITC clone GL-1, E-AB-F0994C) were added and mixed and incubated away from light. Finally, the cells were resuspended and blown for mixing and immediately mounted. The gating strategy was as follows: single cell gate → living cell gate → CD11b + F4/80 + macrophage gate → analysis of co-expression of CD86 and other polarization markers. Single-staining control was used for fluorescence compensation in all experiments, and the positive limit was set using the isotype control (FITC Rat IgG2a, κ).

Mouse spleen tissues were fixed in tissue fixative, dehydrated, permeabilized, embedded, and sliced. The tissue sections underwent antigen retrieval via microwave heating and were subsequently cooled to room temperature. After antigen inactivation and blocking, the sections were incubated with the primary antibody (F4/80 antibody) and iNOS antibody, washed, and incubated with the secondary antibody. After washing, an anti-fluorescence quenching sealing agent containing DAPI was added dropwise, and the cover glass was covered to avoid bubbles. The prepared slides were compressed and stored at 4 °C in the dark, and scanned by the automatic pathological tissue digital scanning imaging system. All experiments were performed in triplicate independently (three biological replicates),

with each biological replicate consisting of three technical replicates. The results were quantitatively calculated using ImageJ. The calculation formula is as follows (Equation (1)):

$$\text{Proportion of INOS}^{+}\text{ cells} = \text{The number of F4/80}^{+}\text{INOS}^{+}\text{ cells/Total cell number of F4/80}^{+} \times 100\% \quad (1)$$

2.4.8. Immunofluorescence Analysis

The cells were inoculated into 24-well plates and cultured for 24 h. Subsequently, cells were treated with different concentrations of SC2-3 for 48 h, and LPS (1 μg/mL) was added to the positive control group. After treatment, the cells were fixed with 4% paraformaldehyde for 15 min, permeabilized with 0.1% Triton X-100 for 10 min (to allow the antibody to enter the cells), and then blocked with 5% BSA for 1 h. It was combined with goat anti-mouse TLR4 (Invitrogen MA5-16216) primary antibody (incubated overnight at 4 °C) and FITC-labeled goat anti-mouse IgG (BOISS bs-0295G-HRP) secondary antibody (incubated in the dark at room temperature for 1 h) and observed and photographed under a fluorescence microscope. The average fluorescence intensity was analyzed by ImageJ software to detect the total TLR4 protein expression level. All experiments were performed in triplicate independently (three biological replicates), with each biological replicate consisting of three technical replicates.

2.4.9. Western Blotting Analysis

The cells were treated with different concentrations of SC2-3 for 48 h. In the experimental group that needed to inhibit TLR4, the TLR4 inhibitor TAK-242 (concentration of 10 μM) was added 1 h before SC2-3 treatment. After treatment, the cells were collected and lysed to extract total protein (lysis buffer was Beyotime RIPA P0013C, protease inhibitor and phosphatase inhibitor were added at 50:1:1). The samples (25 μg protein loading) were separated by SDS-PAGE (80 V 30 min; 120 V 90 min) and then transferred to polyvinylidene fluoride (PVDF) membrane (250 mA 100 min). The primary antibody and secondary antibody were incubated with the membrane in turn, and the images were collected by the Bio-Rad gel imaging analysis system. The primary antibodies used were anti-TLR4 (Invitrogen MA5-16216 1:1000), anti-MyD88 (Proteintech 23230-1-AP 1:10,000), anti-TRAM (TICAM2) (Proteintech; 12705-1-AP 1:1000), anti-TRAF6 (abcam EP592Y 1:1000), anti-NF-κB p-p65 (Affinity; AF2006 1:1000), and anti-GAPDH (Proteintech; 10494-1-AP 1:10,000). All experiments were performed in triplicate independently (three biological replicates), with each biological replicate consisting of three technical replicates.

2.5. In Vivo Immune Activity of SC2-3

2.5.1. Establishment of a Mouse Model of Cyclophosphamide-Induced Immunocompromise

Healthy male C57BL/6J mice, aged 6–8 weeks, weighing 18–22 g, were purchased from SPF (Suzhou) Biotechnology Co., Ltd. (license number: SCXK (Suzhou) 2022-0006, Suzhou, China). All animal procedures were approved by the Shanghai Marine Medical Ethics Committee (ethical batch number: shou-DW-2022-008), and humane care was provided throughout the study. All animals were housed in a temperature-controlled environment under specific pathogen-free (SPF) conditions, with a 12 h light/12 h dark cycle and free access to food and water. During the experimental period, mice were kept in controlled conditions at 25 ± 2 °C, 55–60% humidity, with a normal day/night cycle. Standard diet and water were provided ad libitum. After one week of acclimatization, mice were randomly assigned to six groups (n = 6 per group) using a computer-generated random number table. To ensure blinding during treatment administration, SC2-3 solutions at different concentrations were prepared in identical opaque vials labeled with coded numbers by a researcher not involved in dosing. The investigator administering the treat-

ments was unaware of the group allocations throughout the dosing period. They were given an intraperitoneal injection of CTX (cyclophosphamide, Baxter Oncology GmbH, Halle, Germany, batch no. 34631F) at 80 mg/kg BW/day for modeling for 3 consecutive days. Mice in the CT group were given saline in the same way. The LH group were administered levamisole hydrochloride (LH) 40 mg/kg BW/day (Soleberg Technology Co, Beijing, China) by gavage, while the experimental group SCL, SCM, and SCH received different concentrations of SC2-3 (50 mg/kg BW/day, 100 mg/kg BW/day, and 200 mg/kg BW/day), respectively. Mice in the CT and CTX groups were given an equal volume of saline. Treatments were administered once daily for 14 consecutive days, during which body weights were monitored regularly. After the last administration, the animals were fasted for 12 h. The mice were anesthetized with ether to remove the eyeballs and collect blood. Then the mice were euthanized, and the spleen, thymus, and intestinal tissues were collected for subsequent analysis. Serum and feces samples were frozen at −80 °C for further study. In this study, the volume of gavage was fixed at 200 μL/mouse, which was converted to about 10 mL/kg according to the weight range of mice (18–22 g). All the solutions were filtered by a 0.22 μm microporous membrane to remove bacteria and were used immediately. Short-term storage at 4 °C for no more than 24 h was used to ensure sample stability and activity. We have rigorously enforced blind scoring in histological/IHC analysis to eliminate bias. The specific process is as follows: all slices are randomly coded by researchers who are not involved in the scoring to hide the grouping information; subsequently, the coding slices were independently scored by a researcher who was not aware of the grouping of this study group, according to the scoring criteria; after all the scores are completed, the data is decoded and associated with the original group for statistical analysis.

2.5.2. Spleen and Thymus Indices

At the end of the experiment, the mice were euthanized, and the spleen and thymus from each group were collected and weighed. The weights of the immune organs were recorded, and the immune organ index was calculated using the following Formula (2):

$$\text{Index} = \text{organ weight (mg)}/\text{body weight (g)} \times 10 \quad (2)$$

2.5.3. Blood Cell Analysis

The peripheral blood of mice was collected into EP tubes containing anticoagulants by eyeball removal. The peripheral blood cell indexes were then measured using a three-part automated hematology analyzer (Mindray BC-2800vet).

2.5.4. Measuring the Levels of Expression of TNF-α, IL-1β, IL-6

Whole blood samples were collected from mice by removing the eyeballs, partially stored in enzyme-inactivated centrifuge tubes, and centrifuged at low temperature after standing to obtain serum. The levels of interleukin-6 (IL-6), interleukin-1β (IL-1β), and tumor necrosis factor-α (TNF-α) in mouse serum were detected by ELISA kits (Jingmei, Jiangsu).

2.5.5. H&E Staining Analysis

After euthanizing the mice, the desired tissues were fixed in 4% paraformaldehyde for at least 24 h, followed by paraffin embedding and sectioning. The tissue sections were stained with hematoxylin and eosin (H&E) and subsequently imaged using a digital panoramic slide scanner to facilitate detailed examination of histopathological changes.

2.5.6. Immunohistochemistry Analysis

Spleen and intestinal tissues were fixed in tissue fixative, dehydrated, permeabilized, embedded, sectioned, and prepared for staining. The sections were microwaved for antigen retrieval, then allowed to cool to room temperature. Following antigen inactivation and blocking, the sections were incubated with primary antibodies (IL-6 (GB300007, 1:200), TNF-α (GB15188, 1:300), ZO-1 (GB15195, 1:200), Occludin (GB151401, 1:200), MUC-2 (GB15344, 1:300)). Incubation at 4 °C overnight; antigen repair was performed by microwave method, in which citric acid buffer (pH 6.0) was used for IL-6/TNF-α/MUC-2, and EDTA buffer (pH 9.0) was used for ZO-1/Occludin. HRP-labeled goat anti-rabbit IgG (GB23303) was used as the secondary antibody, and DAB was used for color development at room temperature for 1 h. Finally, the sections were dehydrated and mounted for microscopic examination. The percentage of positive area and integral optical density were analyzed by ImageJ software.

2.5.7. Immunofluorescence Analysis

The spleen tissues embedded in paraffin were dewaxed and hydrated and then washed with distilled water. Subsequently, antigen repair and serum blocking were carried out. Following these preparatory steps, primary antibodies against F4/80 and inducible nitric oxide synthase (iNOS) were applied, and the samples were incubated at 4 °C. After the incubation is completed, add the corresponding secondary antibody and continue the incubation for 50 min. Finally, the cell nuclei were re-stained with DAPI. After sealing the slides, images were acquired using a fluorescence microscope to facilitate detailed analysis.

2.6. Statistical Analysis of Data

All data were expressed as the mean ± standard error of the mean (SEM) from three independent experiments. Normality of data distribution was assessed using the Shapiro–Wilk test, and homogeneity of variances was evaluated by Levene's test. In addition, visual inspection of Q-Q plots and residual plots was performed to confirm the assumptions of ANOVA. For repeated measurement data (e.g., body weight changes), a two-way repeated measures ANOVA was performed with time as the within-subject factor and treatment as the between-subject factor. For comparisons among multiple independent groups, one-way ANOVA was performed, followed by Tukey's HSD post hoc test when the overall ANOVA result was significant ($p < 0.05$). Tukey's HSD was consistently applied for all multiple comparisons to control the family-wise error rate. Statistical analyses were carried out with GraphPad Prism 9.5 and OriginPro 8.5.1; image analysis was performed using NDP.view2. For in vitro experiments, cytokine concentrations (TNF-α, IL-1β, IL-6) were normalized to total protein content measured by BCA assay and expressed as pg per mg of protein. NO and ROS levels were normalized to cell number, with cell counts determined using parallel CCK-8 assays. All normalized data were expressed as fold change relative to the control group. Significance levels were defined as * $p < 0.05$, ** $p < 0.01$, and *** $p < 0.001$.

3. Results

3.1. Isolation and Characterization of SC2-3

The extraction process of glycopeptides from sandworms is shown in Figure 1A. First, crude glycopeptides (SC) were obtained through acetone degreasing followed by extraction with a complex enzyme system, yielding 10.30% (based on the dry weight of the starting material). The crude glycopeptides were then purified using a DEAE-Cellulose column, eluted with 0.2 M and 0.5 M NaCl, producing two main fractions, named SC2 and SC5 (Figure 1B), with yields of 47.0% and 14.6% (relative to the mass of crude glycopeptide loaded), respectively. SC2, the component with the highest yield, was chosen for further

experiments. SC2 was further purified using an S-100 gel filtration column, resulting in the main component SC2-3 with a recovery of 32.4% (based on the mass of SC2 loaded) (Figure 1C). SC2-3 consisted of 54.5% total sugar, 24.1% protein, and 16.4% uronic acid. Additionally, the elution curves for the polysaccharide and protein components of SC2-3 showed overlapping peaks, suggesting that SC2-3 may be a glycoprotein or glycopeptide. To verify this, SC2-3 was analyzed using SDS-PAGE, followed by Coomassie Brilliant Blue and PAS staining. The results showed bands at the same position with both staining methods (Figure 1D). A clear symmetrical peak appeared in the HPGPC chromatogram, indicating that SC2-3 is a homogeneous fraction with a relative molecular weight of about 5061 Da. (Figure 1E). These data, together with the co-elution profile, are consistent with the presence of a glycopeptide complex, suggesting that SC2-3 likely exists as a covalently linked glycopeptide rather than a simple mixture of protein and polysaccharide. However, definitive confirmation of covalent linkage would require further structural evidence, such as mass spectrometric identification of glycopeptide bonds [31].

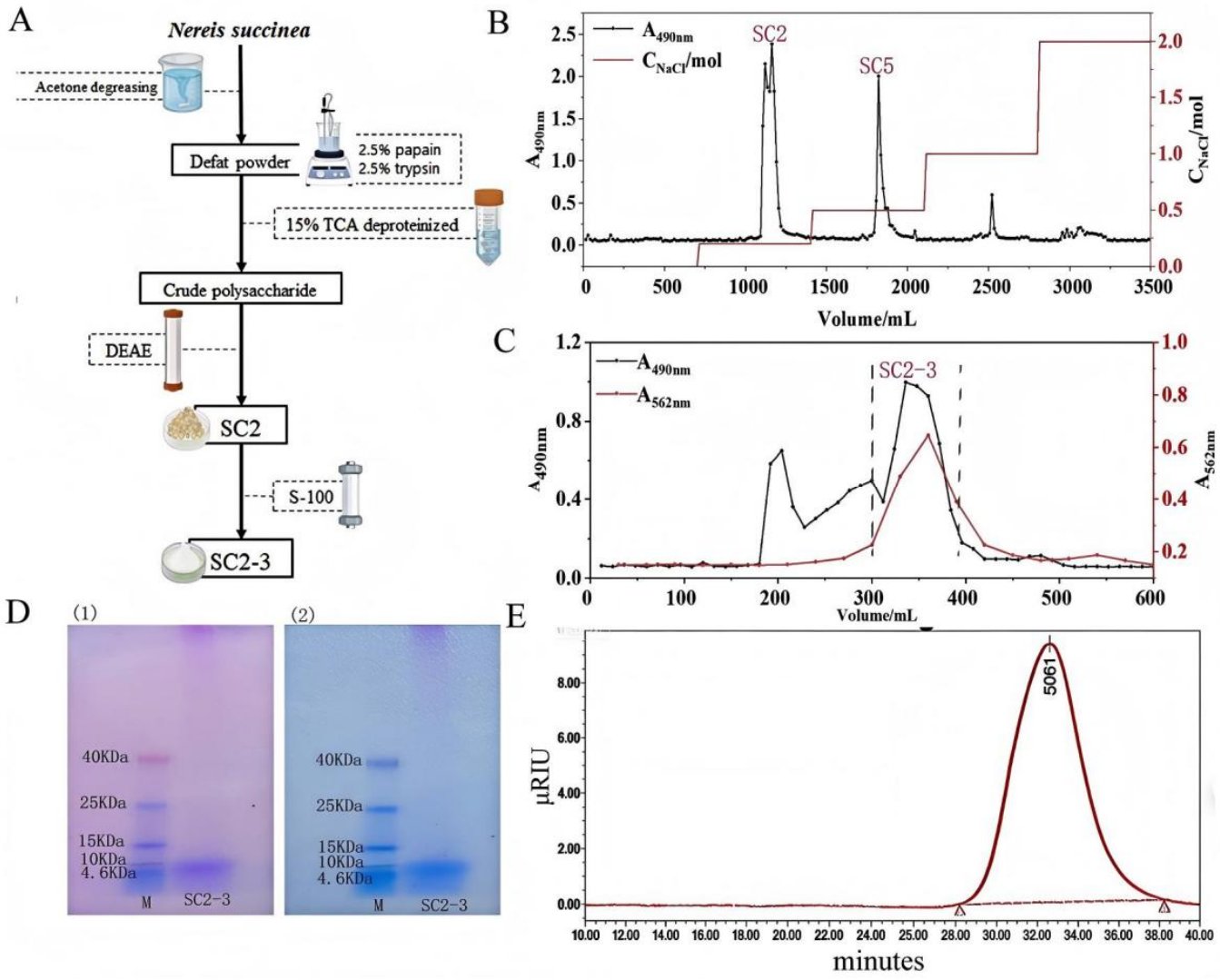


Figure 1. Purification and chemical composition of SC2-3. (**A**) Scheme of isolation and purification of SC2-3 from *Nereis succinea*, (**B**) DEAE Separation chromatogram of SC, (**C**) S-100 Separation chromatogram of SC2, (**D**) SDS-PAGE electrophoretic images of SC2-3 were stained with PAS and Coomassie brilliant blue (Lane: M, molecular weight marker; SC2-3, glycopeptide; (1) PAS staining; (2) Coomassie brilliant blue staining), (**E**) the HPGPC chromatogram of SC2-3.

3.2. Structure Characterization

3.2.1. Monosaccharide Composition and Amino Acid Analysis

The monosaccharide composition of SC2-3 was determined using ion chromatography (Figure S1). SC2-3 mainly consisted of rhamnose (Rha), arabinose (Ara), galactose (Gal), glucosamine (GlcN), glucuronic acid (GlcA), xylose (Xyl), and fucose (Fuc), with smaller amounts of glucose (Glc) and mannose (Man). The corresponding molar ratios are 20.60: 23.96: 9.79: 10.74: 4.85: 7.49: 2.32: 1.79: 2.62. The monosaccharide composition results underscore the structural complexity of the glycan moiety. It is worth noting that the presence of GlcN and Man was detected. While these monosaccharides are commonly found in N-glycan core structures, their presence alone does not confirm the type of glycosylation or glycosidic linkages. Further evidence, such as PNGase F-mediated release of N-glycans (described in Section 3.2.3), is required to verify the presence and structural features of N-glycans.

Amino acids are vital nutrients that support immune cell function during organ development, tissue maintenance, and immune responses [32]. Given that it is a glycopeptide, the amino acid composition of its peptide moiety was additionally determined, and 16 amino acids were identified. The most abundant were glycine (Gly, 14.2%), aspartic acid (Asp, 11.8%), glutamic acid (Glu, 9.75%), and threonine (Thr, 6.1%). Arginine (Arg) was present in smaller amounts (1.3%). Notably, serine, an essential metabolite for cell proliferation, has been shown to promote interleukin-1β (IL-1β) secretion in macrophages through its role in cellular metabolism [33]. Arginine participates in immune functions by stimulating protein synthesis in intestinal cells [34,35]. Amino acid composition analysis showed that SC2-3 contained a variety of essential amino acids, which accounted for 31.8% of the total amino acid content. This composition feature may be related to its observed immunomodulatory activity.

3.2.2. NMR Analysis

To further characterize the structural features of SC2-3, ^{1}H-NMR and ^{13}C-NMR spectra were acquired, as shown in Figure 2A. In the ^{1}H-NMR spectrum, the signals in the chemical shift range of 5.1–4.5 ppm are typical of anomeric protons of sugar rings, while those in the range of 4.0–3.0 ppm correspond to H2–H6 protons of sugar rings. The signals around 7.2 and 6.7 ppm suggest the presence of aromatic amino acid residues, and the peaks around 1–2 ppm are attributed to alkyl protons. The intense signal at 4.8 ppm corresponds to HOD (residual proton signal from the solvent). In the ^{13}C-NMR spectrum, a cluster of peaks around 173 ppm is characteristic of carbonyl carbons (C=O), consistent with the presence of uronic acids or amino acid residues. The signal near 130.0 ppm is typical of aromatic carbons, further supporting the presence of aromatic amino acids. The peaks around 10–20 ppm are attributed to alkyl carbons. These NMR data are consistent with the presence of both carbohydrate and amino acid components in SC2-3, corroborating the results of monosaccharide and amino acid composition analyses. These NMR data are consistent with the presence of both carbohydrate and amino acid components in SC2-3. However, these data do not permit structural identification of glycosidic linkages or peptide sequences. Detailed structural elucidation would require further investigation using advanced NMR techniques.

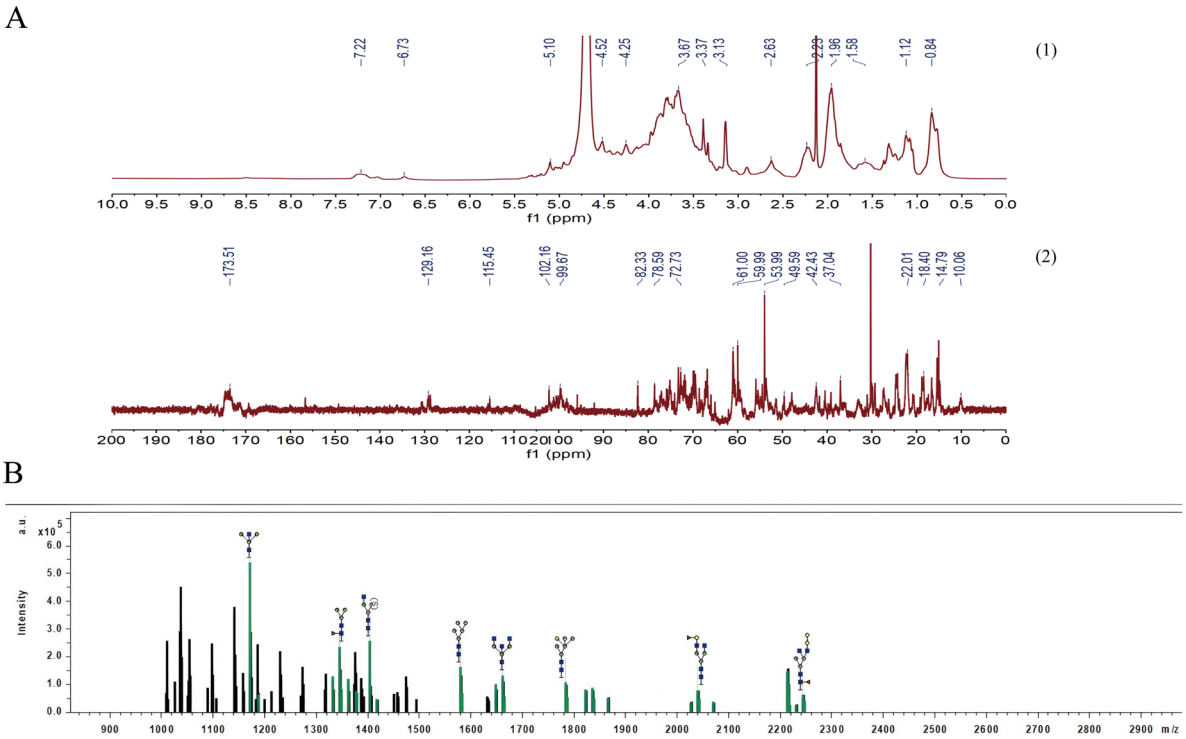


Figure 2. Structural characterization of SC2-3. (**A**) NMR of SC2-3 (**B**) N-glycan analysis of SC2-3 (1. ^{1}H-NMR spectra of SC2-3, 2. ^{13}C-NMR spectra of SC2-3).

3.2.3. N-Glycan Analysis

Currently, research on glycomic analysis of marine-derived glycopeptides is extremely limited, with insufficient supporting data available for reference. Although the glycosylation of marine organisms may be special, PNGase F has been successfully applied to a number of frontier studies of marine invertebrates [36,37]. Herein, we made a preliminary attempt to characterize the N-glycome of SC2-3 using a methodology involving PNGase F-mediated release of N-glycans, permethylation of the released N-glycans, and subsequent detection by MALDI-TOF-MS. Through database matching based on molecular masses, several N-glycan candidate compositions were tentatively assigned. As shown in Figure 2B and Figure S2, the detected N-glycan profiles of SC2-3 include compositions consistent with fucosylated substitutions, and these glycan chains appear relatively shorter compared to typical human N-glycans. Due to the absence of MS/MS fragmentation data, the lack of exoglycosidase digestions, and the lack of orthogonal validation techniques, these data do not permit definitive identification of glycosidic linkages, branching patterns, or anomeric configurations. Consequently, conformational identification of these N-glycans is not possible from the current dataset. Of note, this represents only a preliminary investigation. The analytical methodologies for glycomics of marine-derived glycopeptides and glycoproteins still require further optimization and validation [38].

3.3. Immunological Activity of SC2-3

3.3.1. Cell Viability and Phagocytosis

Macrophages play a central role in the immune system, and their activation is widely recognized as a key regulatory event in initiating and modulating immune responses [39]. The CCK-8 assay was used to assess the effect of SC2-3 on the viability of RAW264.7 macrophages at different concentrations. As shown in Figure 3A, SC2-3 at concentrations from 25 to 1000 μg/mL did not show a clear dose-dependent trend; however, overall cell viability remained above 100%. Compared to the CT group, cell viability was increased,

indicating that SC2-3 was nontoxic and enhanced the metabolic activity of RAW264.7 cells under the tested conditions. Enhanced macrophage phagocytosis speeds up the removal of pathogens such as bacteria, viruses, and fungi, as well as cellular debris, forming the initial line of immune defense. Moreover, increased phagocytic activity allows for more efficient antigen processing and presentation, greatly enhancing the specificity and speed of the adaptive immune response system [40]. As shown in Figure 3B, SC2-3 increased the phagocytic activity of RAW264.7 cells across a concentration range of 50 to 1000 μg/mL, with a stronger effect seen at 800 and 1000 μg/mL. These results indicated that SC2-3 could increase the ability of macrophages to engulf foreign substances, contributing to pathogen defense and potentially strengthening the body's immune response.

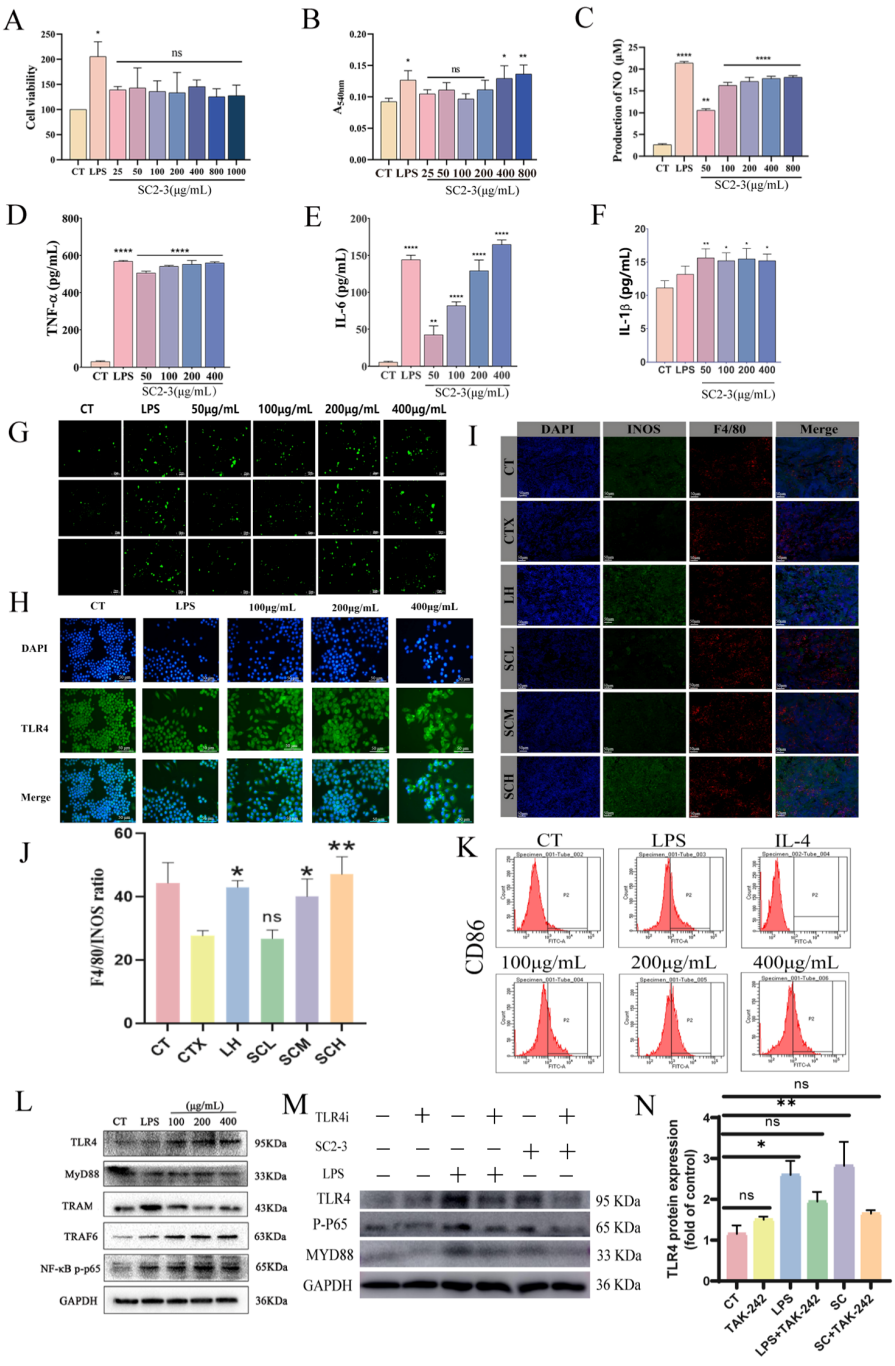


Figure 3. Immune activation effect of SC2-3 in vitro. (**A**) Cell viability of RAW264.7 at different concentrations of SC2-3; (**B**) effects of SC2-3 on phagocytic activity of RAW264.7 cells; (**C**) effects of

SC2-3 on NO secretion in RAW264.7 cells; (**D**–**F**) the effect of SC2-3 on the secretion of TNF-α, IL-6 and IL-1β in RAW264.7 cells; (**G**) effect of SC2-3 on ROS release from RAW264.7 cells (Scale bar = 25 μm); (**H**) effects of SC2-3 on TLR4 protein on RAW264.7 cells (Scale bar = 50 μm); (**I**) immunofluorescence was used to co-stain F4/80 and iNOS in the spleen of mice in each group (n = 6) (Scale bar = 50 μm); (**J**) the proportion of iNOS-positive cells in F4/80-positive macrophages in the spleen of mice in each group (n = 6). (**K**) The effect of SC2-3 on M1 marker CD86 in RAW264.7 cells. (**L**) Expression of TLR4, MyD88, TRAM, TRAF6, and NF-κB p-p65 in RAW264.7 cells in each group; (**M**) SC2-3 activates the TLR4/NF-kB pathway; (**N**) expression level of TLR4 protein. (Data are presented as mean ± SD (n = 3). Statistical significance was determined by one-way ANOVA followed by Tukey's post hoc test. Significance levels were defined as ns (not significant) for $p \geq 0.05$, * for $p < 0.05$. ** for $p < 0.01$, and **** for $p < 0.0001$.

3.3.2. NO and ROS Release

NO is produced during the activation of innate defense immunity [41]. To determine if SC2-3 stimulates NO production in macrophages, the Griess assay was used to measure NO levels in the culture supernatant after 48 h of SC2-3 treatment (Figure 3C). Lipopolysaccharide (LPS, 1 μg/mL) significantly increased NO release, serving as a positive control. SC2-3 also notably elevated NO production in a concentration-dependent manner across the 50–800 μg/mL range. To confirm that the observed NO induction was attributable to SC2-3 itself rather than potential endotoxin contamination, a polymyxin B neutralization assay was performed. As shown in Figure S3, LPS-induced NO production was abrogated by polymyxin B (10 μg/mL) treatment, confirming the neutralizing efficacy under our experimental conditions. In contrast, SC2-3 (800 μg/mL)-induced NO production was not significantly affected by polymyxin B co-treatment. These results demonstrate that the macrophage activation by SC2-3 is intrinsic to the glycopeptide and not due to residual endotoxin.

Reactive oxygen species (ROS) are a crucial part of innate immunity, offering protection against infections [42]. They can directly eliminate invading pathogens and also boost immune responses by activating signaling pathways involved in cytokine and chemokine release by immune cells. As shown in Figure 3G and Figure S4, ROS production steadily increased with higher concentrations of SC2-3, indicating that SC2-3 stimulates ROS generation in a dose-dependent manner.

These results showed that SC2-3 stimulated macrophages to produce NO and ROS in a concentration-dependent manner. Both NO and ROS play critical roles in innate immunity. These suggested that SC2-3 could promote the production of innate immune-related molecules and might have the potential to enhance innate immune responses.

3.3.3. Measurement of TNF-α, IL-1β, and IL-6

In their resting state, macrophages exhibit basic phagocytic activity and the capacity to proliferate. When exposed to foreign stimuli, they become activated and start producing various pro-inflammatory mediators, including interleukins (ILs), interferons (IFNs), tumor necrosis factor-alpha (TNF-α), nitric oxide (NO), and reactive oxygen species (ROS) [43]. Compared to the control group, SC2-3 significantly increased the release of pro-inflammatory cytokines IL-1β, IL-6, and TNF-α in a concentration-dependent manner within the range of 100–400 μg/mL (Figure 3D–F). Notably, the high-concentration SC2-3 group showed a stronger pro-inflammatory effect than the LPS-treated group (1 μg/mL). These results suggest that SC2-3 effectively promoted the expression of inflammatory mediators, activated macrophages, and had a potent immune-enhancing effect.

3.3.4. SC2-3 Promotes an M1-like Activation Profile in Macrophages

Macrophages are important innate immune cells with significant plasticity [44], and their functional phenotypes can be modulated by external stimuli. For instance, LPS is commonly used to induce a pro-inflammatory (M1-like) activation state, while interleukin-4 (IL-4) promotes an anti-inflammatory (M2-like) state in macrophages [45]. In the present study, we assessed the effects of SC2-3 on macrophage activation using the RAW264.7 cell line and mouse splenic macrophages. In RAW264.7 cells, surface marker expression was examined by flow cytometry [46]. As shown in Figure 3K, LPS stimulation increased the mean fluorescence intensity (MFI) of CD86 compared to the CT group, consistent with a shift toward a pro-inflammatory activation state. Treatment with SC2-3 also increased CD86 MFI in a concentration-dependent manner, with the peak shift pattern resembling that of the LPS-treated group, suggesting that SC2-3 promotes a pro-inflammatory activation phenotype in RAW264.7 cells. To further evaluate macrophage activation in an ex vivo context, immunofluorescence double staining for F4/80 (a pan-macrophage marker) and inducible nitric oxide synthase (iNOS, a marker associated with pro-inflammatory activation) was performed on mouse spleen sections (Figure 3I,J). SC2-3 treatment increased the proportion of $iNOS^+$ cells within the $F4/80^+$ macrophage population, indicating that SC2-3 promotes a pro-inflammatory activation profile in splenic macrophages. Taken together, these results indicated that SC2-3 promoted a pro-inflammatory activation state which may be mediated by inducing M1 macrophage polarization.

3.3.5. Immunofluorescence

Toll-like receptors (TLRs), a class of pattern recognition receptors (PRRs), play a vital role in the immune system by acting as key mediators that enable biomacromolecules to activate innate immune responses [47,48]. Among these, TLR4 is highly expressed on the surface of macrophages and is known to initiate downstream signaling cascades upon ligand recognition, ultimately contributing to host defense against pathogens [49]. To further investigate the mechanism of action of SC2-3, the pro-inflammatory role of TLR4 on macrophage surfaces was studied using cellular immunofluorescence. Results showed that TLR4 levels in RAW264.7 cells increased after LPS stimulation compared to the control group (Figure 3H). Compared to the LPS group, green fluorescence on the macrophage surface gradually grew stronger with higher SC2-3 concentrations, peaking at 400 μg/mL. This suggests that SC2-3 significantly boosts TLR4 expression on macrophages at this concentration.

3.3.6. Western Blotting

The NF-κB signaling pathway serves as the main regulatory axis of macrophage-mediated immune and inflammatory responses [31]. The immunomodulatory mechanism of glycopeptide SC2-3 was systematically examined using Western blot analysis (Figure 3L). Compared to the control group, the LPS-treated group showed a significant increase in TLR4, TRAM1, TRAF6, and phosphorylated NF-κB p65 (p-p65), indicating that LPS promotes higher expression of these proteins and activates RAW264.7 cells. Similarly, treatment with SC2-3 elevated the expression of these proteins compared to the control, with levels nearing those seen in the LPS group. To investigate whether SC2-3 specifically regulated the TLR4 pathway, we employed its specific inhibitor, TAK-242. As Figure 3M,N shown, pretreatment with TAK-242 abolished the SC2-3-induced regulation of key downstream signaling molecules, including the upregulation of p-p65 and MyD88 expression, causing their levels to revert to baseline. These results suggested that the immunomodulatory effect of SC2-3 might be mediated through the TLR4 signaling pathway.

3.4. SC2-3 Can Alleviate Cyclophosphamide-Induced Immunosuppression in Mice

3.4.1. The Organ Index and Blood Cell Count

As shown in Figure 4B, the body weight of mice in the CT group steadily increased throughout the experiment. In contrast, mice injected with CTX experienced significant weight loss, accompanied by reduced food intake, lethargy, and slowed movement, indicating immunosuppression. On the 4th day, the mice were treated with SC2-3 glycopeptide and levamisole. On the 6th day, their weight stopped decreasing and began to recover and gradually stabilized on the 12th day.

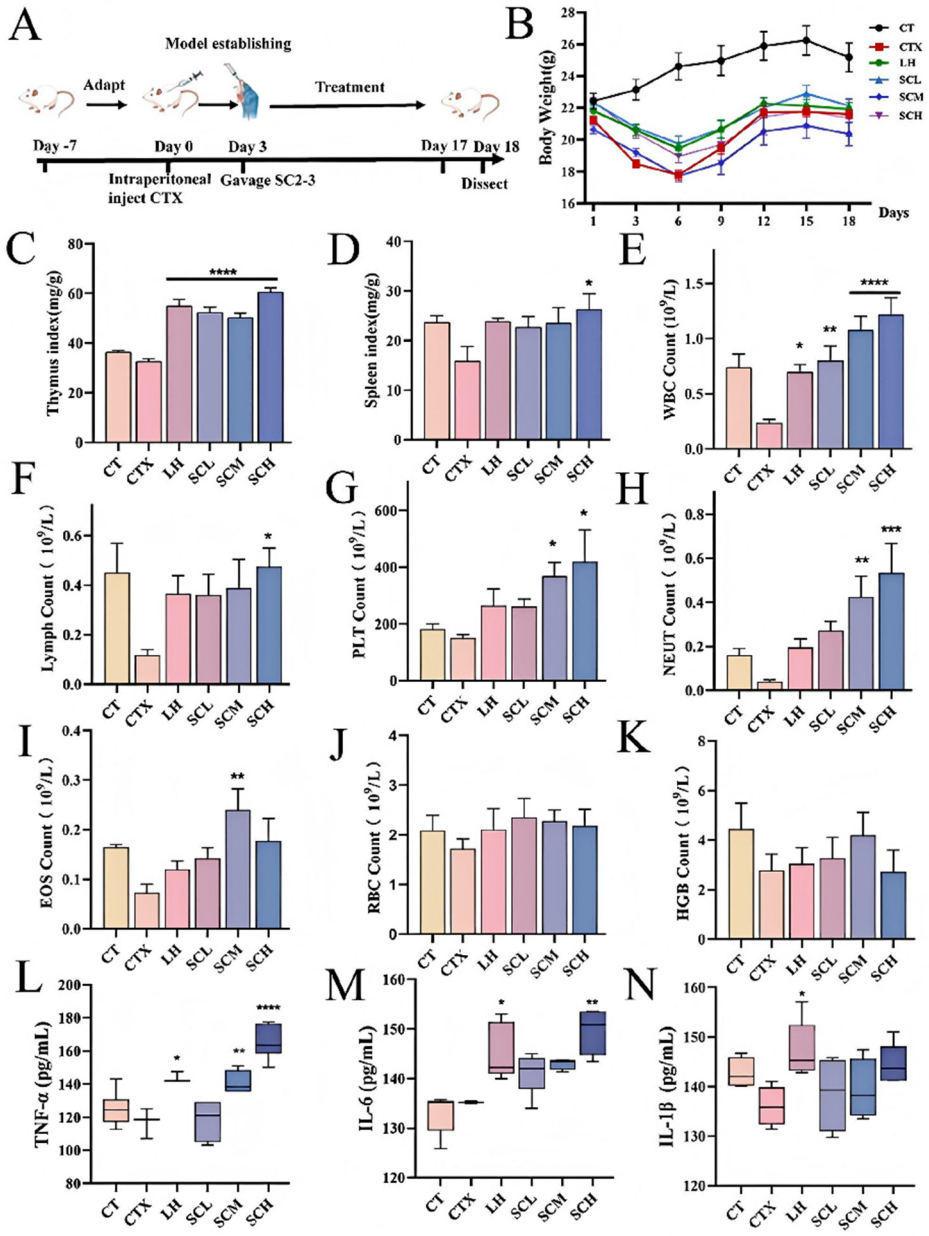


Figure 4. SC2-3 restores CTX-induced immunosuppression in mice (n = 6). (**A**) Dosing regimen for animals; (**B**) effect of glycopeptide SC2-3 on body weight of immunocompromised mice; (**C**,**D**) effect of glycopeptide SC2-3 on immune organs index; (**E**–**K**) improvement of blood cell count in immunocompromised mice mediated by glycopeptide SC2-3. ((**E**): white blood cell count; (**F**): lymphocyte count; (**G**): platelet count; (**H**): neutrophil count; (**I**): eosinophil count; (**J**): red cell count; (**K**): hemoglobin count); (**L**–**N**) the effect of SC2-3 on the levels of inflammatory factors in serum of immunosuppressed

mice. (Data are presented as mean ± SEM (n = 6 per group). Statistical significance was determined by one-way ANOVA followed by Tukey 's post hoc test. Significance levels were defined as ns (not significant) for $p \geq 0.05$, * for $p < 0.05$. ** for $p < 0.01$, *** for $p < 0.001$, and **** for $p < 0.0001$).

Immune organs are important organs that perform immune regulatory functions in the body, and their activities are closely related to the changes in the immune organ index [50]. As shown in Figure 4C,D, the thymus and spleen indices in the CTX group were significantly lower than those in the normal group, indicating that CTX caused atrophy of immune organs and led to immune dysfunction in mice. Compared to the control group, treatment with the polysaccharide restored both thymus and spleen indices toward normal levels, with the thymus index showing a dose-dependent increase. Additionally, the spleen indices of mice in the LH, SCL, SCM, and SCH groups were significantly higher.

As shown in Figure 4E–K, compared to the control (CT) group, the CTX group showed decreases in leukocytes, platelets, neutrophils, lymphocytes, hemoglobin, and eosinophils. After treatment with LH and SC2-3, counts of white blood cells, platelets, neutrophils, and lymphocytes in peripheral blood increased in a dose-dependent manner, with the SCH group demonstrating the most significant effects (Figure 4E–H). Although the levels of red blood cells and hemoglobin did not show a significant dose-dependent trend, compared with the CTX group, these two parameters showed a trend of recovery to the control level after SC2-3 treatment. (Figure 4J,K). Additionally, eosinophil counts rose with both LH and SC2-3 treatments, with the SCM group showing the greatest increase, surpassing both the SCL and SCH groups (Figure 4I).

3.4.2. Cytokine Secretion

Immune-related cytokine levels in mouse serum were measured using ELISA (Figure 4L–N). Compared to the CT group, the CTX group showed significant reductions in serum TNF-α, IL-1β, and IL-6 levels, confirming the successful establishment of the immunosuppression model. Treatment with LH and the glycopeptide significantly increased these cytokine levels in the serum, with the high-dose groups showing the most pronounced effects.

3.4.3. H&E Staining

The immune system consists of immune organs, cells, and active substances, serving as an effective defense against viruses and microorganisms from outside. The spleen and thymus are the main peripheral and central immune organs, respectively, where immune cells mature. As shown in Figure 5A, spleen tissue sections from mice were stained with hematoxylin and eosin (HE) to evaluate the effects of SC2-3. In the control group, splenic follicles were well organized, with a clear boundary between the red and white pulp. The splenic cords in the red pulp remained intact, and blood cells around the follicles were evenly distributed. Compared to the CT group, splenic follicles in the CTX group were poorly formed, with blurred and partially merged boundaries between the red and white pulp. Following treatment with LH and SC2-3, the structure of the splenic follicles improved, and the boundary between the red and white pulp became clearer. After treatment with 50 mg/kg SC2-3, the overall structure of the splenic follicles was visible, although most had unclear boundaries between the red and white pulp. As the SC2-3 dose increased, cell density improved, the white pulp became more distinct, and clear boundaries between the red and white pulp were observed, with follicles separated. Notably, spleen morphology in the high-dose SC2-3 group (200 mg/kg) resembled that of the control group, indicating that SC2-3 at higher doses can effectively restore spleen tissue to a normal state, demonstrating its reparative effect on damaged spleen tissue.

As shown in Figure 5B, H&E staining of the mouse thymus was used to assess the effect of the glycopeptide on cyclophosphamide-induced thymic injury. In the control group, the boundary between the cortex and medulla was clear, with thymic corpuscles easily visible in the medulla. However, after cyclophosphamide injection, the cortical and medullary structures in the CTX group appeared diffuse; thymic corpuscles were sparse or absent, and the tissue staining was lighter. Following glycopeptide treatment, the cortical and medullary architecture gradually became clearer and returned to a normal appearance.

To evaluate the effect of SC2-3 on colon pathology in CTX-treated mice, hematoxylin and eosin (H&E) staining was conducted (Figure 5C). Histological analysis showed that villi in the CT group were intact, slender, and closely packed. In contrast, CTX treatment led to intestinal epithelial damage, characterized by shortened, thickened, and disorganized villi, along with cell shedding, vacuolation, and loss of integrity at the villus tips. After glycopeptide treatment, epithelial damage was reduced, and the villi appeared more intact and densely packed.

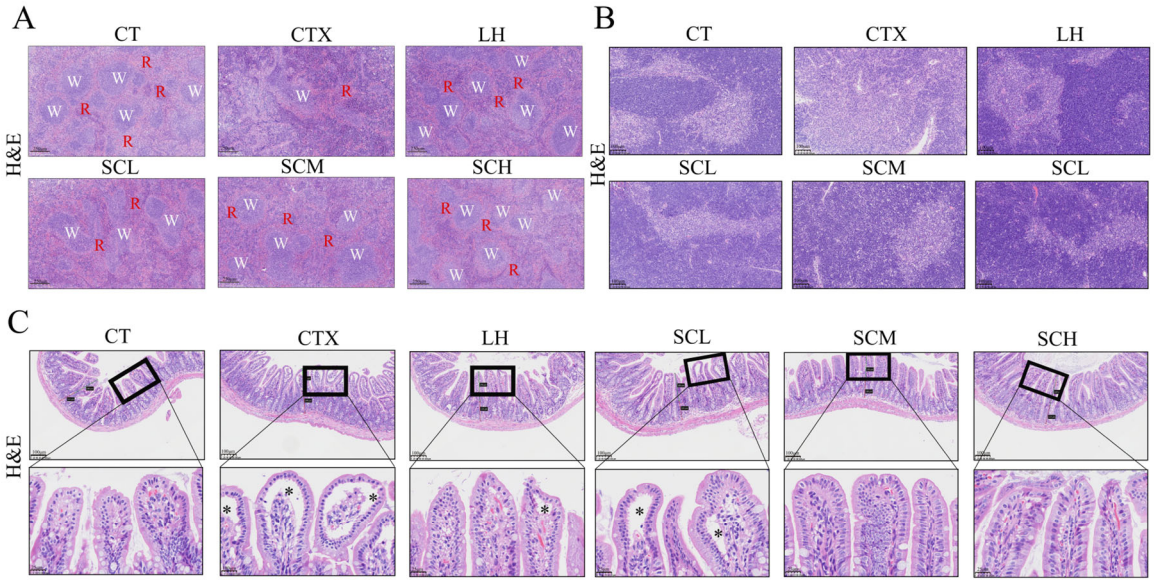


Figure 5. SC2-3 restored CTX-induced thymus and spleen damage in mice (n = 6). (**A**) H&E staining of spleen (R is red pulp; W is white pulp (Scale bar = 100 μm)); (**B**) H&E staining of thymus (Scale bar = 100 μm); (**C**) protective effect of SC2-3 on intestinal barrier damage in CTX-treated mice (Scale bars: 100 μm (above), 25 μm (below); * Symbol indicates the vacuoles in intestinal epithelial cells.). (Note: All slices were randomly coded to hide the grouping, scored independently by researchers who were not aware of the grouping, decoded before statistics, and associated with the original grouping).

3.4.4. Immunohistochemistry Analysis

To further verify the restorative effect of this glycopeptide on chemotherapy-induced immunosuppression in vivo, corresponding immunohistochemical experiments were conducted. First, we measured the expression levels of IL-6 and TNF-α in the spleen. Both cytokines were significantly decreased in the CTX group compared to the control group, but increased notably after treatment with SC2-3 and LH. Immunohistochemical analysis showed that SC2-3 enhances IL-6 and TNF-α expression in the spleen (Figure 6A,C,D). Given that IL-6 and TNF-α are downstream cytokines regulated by the NF-κB pathway, these results suggest that the observed immunomodulatory effects of SC2-3 may be associated with NF-κB-mediated signaling. However, definitive confirmation of NF-κB pathway activation would require direct assessment of upstream signaling events such as IκBα degradation or p65 nuclear translocation.

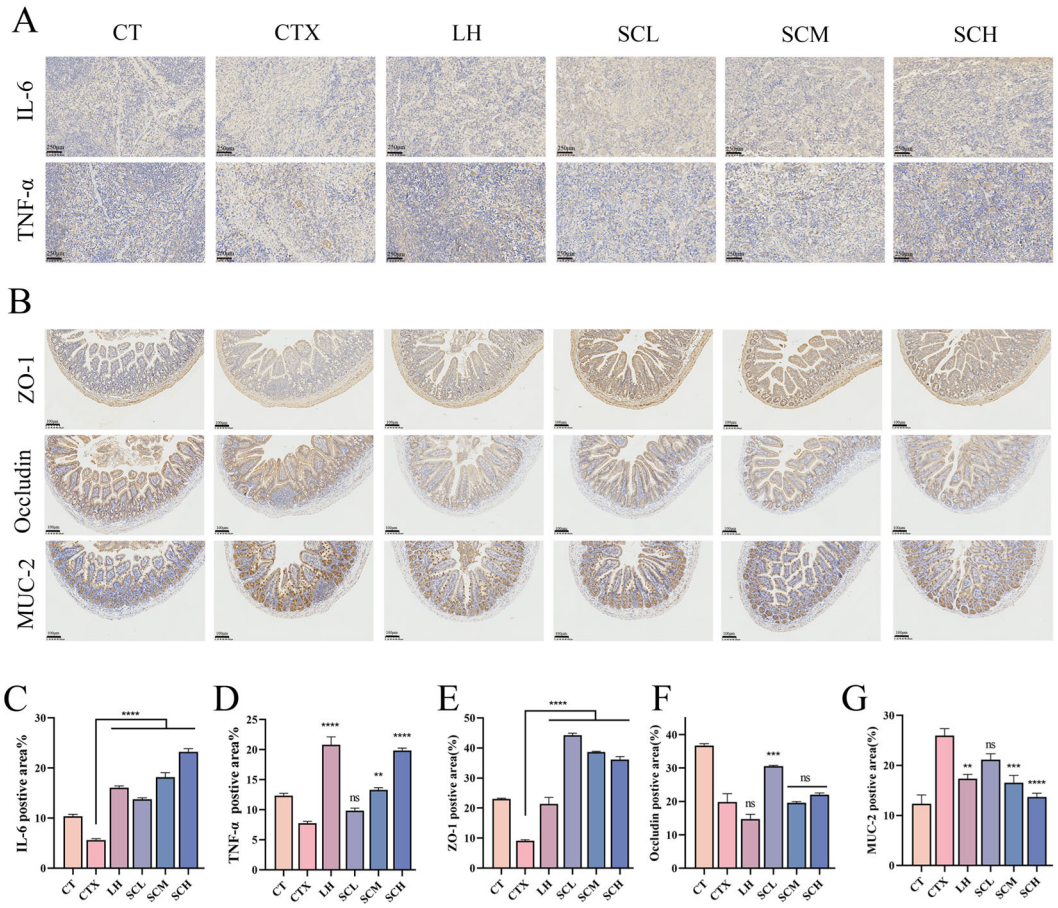


Figure 6. Immunohistochemical analysis of SC2-3 on spleen and intestinal-related indices in CTX-induced immunocompromised mice. (n = 6) (**A**) Immunohistochemical analysis of IL-6 and TNF-α in the spleen; (**B**) immunohistochemical analysis of ZO-1, Occludin and MUC-2 in the intestines; (**C**) statistical chart of IL-6; (**D**) statistical chart of TNF-α; (**E**) statistical chart of ZO-1; (**F**) statistical chart of Occludin; (**G**) statistical chart of MUC-2. (Statistical significance was determined by one-way ANOVA followed by Tukey's post hoc test. Significance levels were defined as ns (not significant) for $p \geq 0.05$, ** for $p < 0.01$, *** for $p < 0.001$, and **** for $p < 0.0001$.) (Note: All slices were randomly coded to hide the grouping, scored independently by researchers who were not aware of the grouping, decoded before statistics, and associated with the original grouping).

Secondly, we examined the effect of SC2-3 on the expression of intestinal tight junction proteins and MUC-2, which are essential for maintaining the integrity of the intestinal barrier. Compared to the control group, the CTX group showed a significant reduction in ZO-1 and occludin expression levels (Figure 6B,E–G), indicating that cyclophosphamide damaged the intestinal epithelium. After glycopeptide treatment, the levels of occludin and ZO-1 were significantly increased, suggesting a protective effect on the intestinal barrier. In the CTX group, MUC-2 protein expression was elevated, while ZO-1 and occludin expression were decreased. These changes are consistent with disruption of intestinal epithelial integrity, suggesting potential impairment of the intestinal barrier. The observed upregulation of MUC-2 might represent a compensatory response of goblet cells to reinforce the protective mucus layer.

4. Discussion

Marine organisms, as a treasure trove of bioactive substances, have attracted increasing attention for their diverse glycoconjugates with unique structural features and biological activities [15]. In this study, we successfully isolated and purified a glycopeptide, designated

SC2-3, from *Nereis succinea*, a marine annelid with a long history of medicinal and edible use in East Asia. Comprehensive structural characterization combined with systematic in vitro and in vivo evaluation of immunomodulatory activity provides valuable insight into the potential of marine glycopeptides as naturally derived dietary supplements.

Structural characterization is fundamental to understanding the biological activities of glycopeptides, as the interplay between carbohydrate and peptide moieties often dictates their functional properties [17]. SC2-3 was identified as a homogeneous glycopeptide with a molecular weight of 5061 Da. The overlapping peaks of polysaccharide and protein in its elution profile, combined with positive staining by both Coomassie Brilliant Blue and Schiff reagent in SDS-PAGE, provide strong evidence that SC2-3 is a glycopeptide complex, likely with covalent linkages between the glycan and peptide moieties [51]. While these data support this interpretation, definitive proof of covalent conjugation would require additional analytical approaches. Such structural integration is critical for its bioactivity, as both sugar and peptide moieties may synergistically contribute to interactions with immune cells. In this study, N-glycans were released using PNGase F for profiling. Considering the potentially unique glycosylation in marine annelids, future work could employ orthogonal methods (e.g., PNGase A or chemical release) to obtain a more complete glycan profile and elucidate the fine structural details of these modifications.

Macrophages, as central players in innate immunity, exhibit remarkable plasticity and are critical for initiating and regulating immune responses [46]. SC2-3 significantly enhanced macrophage function through multiple pathways, including promoting the proliferation and phagocytic activity of RAW264.7 macrophages, increasing the production of NO and ROS, and upregulating the secretion of pro-inflammatory cytokines (IL-1β, TNF-α, and IL-6) [40,41,52]. A key observation was that SC2-3 promoted an M1-skewed activation profile in macrophages, as evidenced by the upregulation of the surface marker CD86 and an increased proportion of $F4/80^{+}iNOS^{+}$ cells in mouse spleen tissues. While these two markers are indicative of M1-like activation, a comprehensive characterization of macrophage polarization would require assessment of a broader panel of markers, including pro-inflammatory cytokines (e.g., IL-12, TNF-α) for M1 and anti-inflammatory markers (e.g., CD206, Arg1, IL-10) for M2. M1 macrophages exhibit a characteristic pro-inflammatory phenotype and contribute to both innate and adaptive immune responses by secreting pro-inflammatory cytokines and enhancing antigen presentation. In the case of CTX-induced immunosuppression, this enhanced pro-inflammatory activity may help restore immune function and strengthen the host's defense against infection. However, it is worth noting that excessive or prolonged M1 polarization can lead to tissue damage and chronic inflammation [44]. Therefore, the immunomodulatory effects of SC2-3 should be explained in a balanced framework: although its ability to promote pro-inflammatory activation is beneficial to counteract immunosuppression, the safety and potential adverse effects of this activation need further study. Future studies should monitor markers of inflammation-related tissue damage to establish a comprehensive SC2-3 safety profile. Mechanistically, Western blot and immunofluorescence analyses confirmed that SC2-3 activates the TLR4/NF-κB signaling pathway, as indicated by elevated expression of TLR4, TRAM1, TRAF6, and phosphorylated NF-κB p65. These findings suggest that SC2-3 may exert its immunomodulatory effects through the TLR4/NF-κB pathway. TLR4 is a key PRR expressed on macrophages. Activation of the TLR4/NF-κB pathway is consistent with the observed increase in pro-inflammatory cytokines and M1 polarization, as this pathway is a well-established regulator of macrophage-mediated inflammatory responses [21,53]. These findings suggest that SC2-3 may serve as a potential TLR4 agonist candidate. While this property could benefit immunosuppressed states, strong TLR4 activation poses safety concerns in humans, including risks of chronic inflammation and tissue damage upon

prolonged exposure. Therefore, future studies must evaluate dose–response, chronic toxicity, and inflammatory pathology to establish a safety profile. At present, our findings provide mechanistic insights, but practical application as a dietary supplement requires rigorous safety validation [54].

CTX, a widely used chemotherapeutic agent, causes severe immunosuppression by damaging immune organs, reducing blood cell counts, and impairing cytokine secretion [50]. Our in vivo studies demonstrated that SC2-3 effectively mitigates these CTX-induced adverse effects. Treatment with SC2-3 dose-dependently increased spleen and thymus indices, indicating restoration of immune organ function. Immune organs are critical for immune cell maturation and proliferation, and their atrophy is a hallmark of immunosuppression [50]. Additionally, SC2-3 reversed CTX-induced reductions in white blood cells, platelets, lymphocytes, and neutrophils, which are essential for pathogen defense and tissue repair. The recovery of serum cytokine levels (IL-1β, TNF-α, IL-6) further confirms SC2-3's immune-enhancing effect. However, it is important to critically evaluate the potential implications of restoring these pro-inflammatory cytokines [43]. In this study, SC2-3 elevated cytokines to levels facilitating immune recovery, and histopathological examination revealed no inflammation-related tissue damage (Figures 5 and 6), suggesting SC2-3 does not induce a hyperinflammatory state. Nevertheless, future studies should include long-term safety assessments to fully exclude potential pro-inflammatory risks. This study suggests that the role of SC2-3 is to help the immune system restore balance from CTX inhibition, rather than causing excessive inflammation. Histopathological analysis revealed that SC2-3 repairs CTX-damaged spleen, thymus, and intestinal tissues. In the spleen, SC2-3 restored the structure of splenic follicles and the boundary between red and white pulp, which are critical for antigen presentation and lymphocyte activation. In the intestine, SC2-3 upregulated the expression of tight junction proteins (ZO-1 and Occludin) and normalized MUC-2 levels, maintaining intestinal barrier integrity. The intestinal barrier is a critical component of mucosal immunity, and its dysfunction can lead to increased permeability and systemic inflammation [34]. By protecting the intestinal barrier, SC2-3 may indirectly support systemic immune homeostasis, highlighting its multifaceted role in immune regulation. A key limitation is that SC2-3 (~5 kDa) exceeds the typical cutoff for passive intestinal absorption, making intact absorption unlikely. Therefore, its systemic immunomodulatory effects, such as restoring spleen function and elevating serum cytokines, are likely mediated locally in the gut. SC2-3 may interact with intestinal epithelial cells or gut-associated lymphoid tissue via pattern recognition receptors (e.g., TLR4), or modulate gut microbiota composition, triggering signaling cascades that propagate systemic effects. These mechanisms remain speculative, as the current study did not assess intestinal absorption, local immune activation, or microbiota changes. Future studies using intestinal co-culture systems, labeled-compound pharmacokinetics, and microbiota profiling are needed to clarify these mechanisms.

This study expands the current understanding of marine glycopeptides by demonstrating the immunomodulatory potential of *Nereis succinea*-derived SC2-3. Unlike previous studies focusing on glycopeptides from sea cucumbers or brown algae [15], our work highlights *Nereis succinea* as a new source of bioactive glycoconjugates, promoting its high-value utilization. This study provides a scientific foundation for future investigations into *Nereis* glycopeptide-based immunomodulatory products. However, it should be emphasized that the current findings are preliminary from a translational perspective. Further studies, including dedicated toxicity assessments and long-term safety evaluations, are needed to confirm its safety profile [54].

5. Conclusions

SC2-3, a glycopeptide isolated from *Nereis succinea*, exhibited potent immunostimulatory effects in vitro by promoting an M1-like activation profile in macrophages, an effect associated with the TLR4 signaling pathway. In vivo, SC2-3 effectively mitigated CTX-induced immunosuppression by restoring immune organ function, increasing peripheral blood cell counts, and modulating cytokine secretion profiles in vivo. These results indicated SC2-3 as a potential bioactive molecule for a marine-derived immunomodulatory agent, warranting further investigation, including safety and toxicological studies. Its demonstrated capacity to partially restore selected immune parameters suggested its potential to bolster immune function and ameliorate immunosuppressive conditions, warranting further investigation.

Supplementary Materials: The following supporting information can be downloaded at: https://www.mdpi.com/article/10.3390/foods15050874/s1, Figure S1: Monosaccharide composition of SC2-3; Figure S2: N-glycome mass spectrometry analysis of SC2-3; Figure S3: Effect of polymyxin B on SC2-3-induced NO production in RAW264.7 cells; Figure S4: ROS fluorescence quantification.

Author Contributions: Y.L.: conceptualization, investigation, formal analysis, and writing—original draft. Y.H.: conceptualization, investigation, formal analysis, and writing—original draft. J.L.: methodology and investigation. Y.Z.: funding acquisition, supervision, and writing—review and editing. P.W.: funding acquisition, supervision, and writing—review and editing. All authors have read and agreed to the published version of the manuscript.

Funding: This work was supported by the Fund of the Technology Innovation Center for Exploitation of Marine Biological Resources, MNR, (TICMBR202506), the Open Project Fund of Guangdong Provincial Key Laboratory of Green Processing of Natural Products and Product Safety (202502), and the Open Project Fund of Marine Biomedical Science and Technology Innovation Platform of Lin-Gang Special Area (RWS-2024-002).

Institutional Review Board Statement: The animal study protocol was approved by Animal Ethics Committee of Shanghai Ocean University (protocol code SHOU-DW-2025-038 and approval date: 28 February 2025).

Informed Consent Statement: Not applicable.

Data Availability Statement: All data needed to evaluate the conclusions are present in the paper. Additional data related to this paper may be requested from the authors.

Conflicts of Interest: The authors report no conflicts of interest.

References

1. Liu, C.; Shen, M.; Liu, Y.; Manhas, A.; Zhao, S.R.; Zhang, M.; Belbachir, N.; Ren, L.; Zhang, J.Z.; Caudal, A. CRISPRi/a screens in human iPSC-cardiomyocytes identify glycolytic activation as a druggable target for doxorubicin-induced cardiotoxicity. *Cell Stem Cell* **2024**, *31*, 1760–1776.e9. [CrossRef] [PubMed]
2. Vo, J.B.; Ramin, C.; Veiga, L.H.; Brandt, C.; Curtis, R.E.; Bodelon, C.; Barac, A.; Roger, V.L.; Feigelson, H.S.; Buist, D.S. Long-term cardiovascular disease risk after anthracycline and trastuzumab treatments in US breast cancer survivors. *JNCI J. Natl. Cancer Inst.* **2024**, *116*, 1384–1394. [CrossRef] [PubMed]
3. Nagai-Singer, M.A.; Wambogo, E.A.; Pasiakos, S.M.; Gahche, J.J. Prepandemic prevalence of dietary supplement use for immune benefits. *JAMA Netw. Open* **2025**, *8*, e2459291. [CrossRef]
4. Ulery, J.A.; Melton, B.; Bland, H.; Riggs, A.J. Understanding the scientific evidence and regulatory state of the US dietary supplement industry: Considerations for health and fitness practitioners. *Strength Cond. J.* **2021**, *43*, 87–94. [CrossRef]
5. Frenkel, M.; Mathis, S.E. Diet, Nutrition, supplements, and integrative oncology in cancer care. *Nutrients* **2025**, *17*, 3422. [CrossRef]
6. Basak, S.; Gokhale, J. Immunity boosting nutraceuticals: Current trends and challenges. *J. Food Biochem.* **2022**, *46*, e13902. [CrossRef]
7. Skenderidou, I.; Leontopoulos, S.; Skenderidis, P. Functional food ingredients enhancing immune health: A systematic review. *Int. J. Mol. Sci.* **2025**, *26*, 8408. [CrossRef]

8. Wan, X.; Yin, Y.; Zhou, C.; Hou, L.; Cui, Q.; Zhang, X.; Cai, X.; Wang, Y.; Wang, L.; Tian, J. Polysaccharides derived from chinese medicinal herbs: A promising choice of vaccine adjuvants. *Carbohydr. Polym.* **2022**, *276*, 118739. [CrossRef]
9. Yang, Y.; Li, H.; Wang, F.; Jiang, P.; Wang, G. An arabinogalactan extracted with alkali from portulaca oleracea L. used as an immunopotentiator and a vaccine carrier in its conjugate to BSA. *Carbohydr. Polym.* **2023**, *316*, 120998. [CrossRef]
10. Xu, M.; Jiang, Z.; Ren, J.; Zhou, S.; Zhang, X.; Wu, W.; Li, H.; Li, B.; Wang, J.; Jiao, L. De-starched panax ginseng polysaccharide: Preparation, in vitro digestion, fermentation properties and the activating effect of the resultant products on RAW264.7 cells. *Carbohydr. Polym.* **2025**, *351*, 123103. [CrossRef]
11. Zhao, H.; Liu, L.; Liu, N.; Deng, B.; Li, M.; Li, D.; Ji, L.; Wang, G.; Yang, F. Laetiporus sulphureus polysaccharides ameliorate chronic alcoholic liver disease by activating p62/Nrf2, AMPK pathways and reshaping gut microbiota. *Food Sci. Hum. Wellness* **2024**, 9250405. [CrossRef]
12. Sun, Y.; Men, Q.; Ren, X.; Guo, X.; Song, S.; Ai, C. Scytosiphon lomentaria fucoidan alleviates alcohol-induced liver injury in mice via the modulation of gut microbiota and bile acid-FXR/AMPK and NF-κB pathways. *Food Sci. Hum. Wellness* **2024**, 9250345. [CrossRef]
13. Ou, J.; Liu, X.; Chen, J.; Huang, H.; Jia, X.; Xu, B.; Yu, Z.L.; Zhong, S. Attenuation of arsenic-induced gut injury in mice by sulfated glycosaminoglycan from swim bladder via regulation of gut microbiota, metabolites, and intestinal barrier integrity. *Food Sci. Hum. Wellness* **2024**, *14*, 9250248. [CrossRef]
14. Lu, X.W.; Qin, S.; Wang, Q.; Lu, C.Y.; Li, W.J. Functional activity and mechanisms of common marine traditional chinese medicine. *Food Med. Homol.* **2025**, *2*, 9420075. [CrossRef]
15. Lu, X.; Huang, L.; Chen, J.; Ou, Y.; Wu, J.; Bodjrenou, D.M.; Hu, J.; Zhang, Y.; Farag, M.A.; Guo, Z. Marine glycoproteins: A mine of their structures, functions and potential applications. *Crit. Rev. Food Sci. Nutr.* **2024**, *64*, 9191–9209. [CrossRef]
16. Hasin, O.; Shoham, S.; Kashman, Y.; Ilan, M.; Carmeli, S. Theonellamides j and k and 5-cis-apoa-theopalauamide, bicyclic glycopeptides of the red sea sponge *Theonella swinhoei*. *Mar. Drugs* **2021**, *20*, 31. [CrossRef]
17. Wang, D.; Zhang, B.; Ren, L.; Jiang, Y.; Meng, Y.; Ma, R.; Wang, S.; Li, X.; Cui, F.; Li, T. Structure, sources, functional mechanisms, and applications of bioactive glycopeptides in food: A comprehensive review. *Trends Food Sci. Technol.* **2025**, *157*, 104899. [CrossRef]
18. Wang, H.; Xu, S.; Li, D.; Xie, Z. Structural characterization and macrophage polarization-modulating activity of a novel polysaccharide from large yellow tea. *J. Agric. Food Chem.* **2022**, *70*, 12565–12576. [CrossRef] [PubMed]
19. Hu, G.; Shao, T.; Wang, J.; Zhang, H.; Shang, X.; Liu, C.; Wu, J.; Lv, Q.; Zhou, Y.; Chen, L.; et al. Structural characterization of a branched polysaccharide isolated from thesium chinense turcz. and its ameliorative effects on ulcerative colitis. *J. Agric. Food Chem.* **2025**, *73*, 26154–26171. [CrossRef]
20. Yang, Y.; Wu, H. Immunomodulatory function and anti-tumor mechanism of natural polysaccharides: A review. *Front. Immunol.* **2023**, *14*, 1147641. [CrossRef] [PubMed]
21. Xing, Y.; Zheng, Y.; Zhang, J.; Chen, L.; Xu, Y.; Jin, X.; Hong, L.; Yan, S.; Shi, B. Purification, characterization, and potential Immune-regulation mechanism of polysaccharides from artemisia odosica krasch. *Molecules* **2025**, *30*, 675. [CrossRef]
22. Tao, L.; Yin, Y.; Qing, W.S.; Jian, Y.L. Nutritional analysis and food safety study of perinereis aibuhitensis. *J. Appl. Oceanogr.* **2016**, *35*, 412–417.
23. Lavigne, G.J.; Khoury, S.; Abe, S.; Yamaguchi, T.; Raphael, K. Bruxism physiology and pathology: An overview for clinicians. *J. Oral Rehabil* **2008**, *35*, 476–494.
24. Zhu, G.; Chen, Z.; Ye, N. Determination of nutritional components of cultured perinereis aibuhitensis in zhanjiang. *Curr. Fish* **2014**, *39*, 76–77.
25. Zhang, G.; Li, H.; Liu, S.; Lu, M.; Tang, L.; Sun, L. Preparation of nereid oligopeptide and investigation of the mechanism underlying the induction of apoptosis in human lung cancer H1299 cells. *Mol. Med. Rep.* **2022**, *25*, 194. [CrossRef]
26. Wu, R.; Patocka, J.; Nepovimova, E.; Oleksak, P.; Valis, M.; Wu, W.; Kuca, K. Marine invertebrate peptides: Antimicrobial peptides. *Front. Microbiol.* **2021**, *12*, 785085. [CrossRef]
27. Zheng, Y.; Ding, G.; Yang, Z.; Yu, F.; Jia, Y.; Wu, Z.; Chen, R. Enzymatic preparation and antithrombotic activity of anticoagulant peptides from perinereis aibuhitensis. *Food Sci.* **2017**, *38*, 171–177.
28. Wang, Y.; Jing, Y.; Leng, F.; Wang, S.; Wang, F.; Zhuang, Y.; Liu, X.; Wang, X.; Ma, X. Establishment and application of a method for rapid determination of total sugar content based on colorimetric microplate. *Sugar Tech.* **2017**, *19*, 424–431. [CrossRef]
29. Blumenkrantz, N.; Asboe-Hansen, G. New method for quantitative determination of uronic acids. *Anal. Biochem.* **1973**, *54*, 484–489. [CrossRef] [PubMed]
30. Wang, P.; Zhang, L.; Yao, J.; Shi, Y.; Li, P.; Ding, K. An arabinogalactan from flowers of panax notoginseng inhibits angiogenesis by BMP2/Smad/Id1 signaling. *Carbohydr. Polym.* **2015**, *121*, 328–335. [CrossRef]
31. Lu, X.; Dai, Y.; Yang, S.; Fu, T.; He, Y.; Zeng, F.; Chen, T.; Cao, Y.; Li, R.; Li, J. Purification and characterization of a glycoprotein from sipunculus nudus and its immune-enhancing activity to RAW 264.7 macrophages. *Food Res. Int.* **2023**, *174*, 113591. [CrossRef]

32. Yang, L.; Chu, Z.; Liu, M.; Zou, Q.; Li, J.; Liu, Q.; Wang, Y.; Wang, T.; Xiang, J.; Wang, B. Amino acid metabolism in immune cells: Essential regulators of the effector functions, and promising opportunities to enhance cancer immunotherapy. *J. Hematol. Oncol.* **2023**, *16*, 59. [CrossRef]
33. Madeo, F.; Carmona-Gutierrez, D.; Hofer, S.J.; Kroemer, G. Caloric restriction mimetics against age-associated disease: Targets, mechanisms, and therapeutic potential. *Cell Metab.* **2019**, *29*, 592–610. [CrossRef]
34. Bertrand, J.; Goichon, A.; Déchelotte, P.; Coëffier, M. Regulation of intestinal protein metabolism by amino acids. *Amino Acids* **2013**, *45*, 443–450. [CrossRef] [PubMed]
35. Tan, B.; Yin, Y.; Kong, X.; Li, P.; Li, X.; Gao, H.; Li, X.; Huang, R.; Wu, G. L-Arginine stimulates proliferation and prevents endotoxin-induced death of intestinal cells. *Amino Acids* **2010**, *38*, 1227–1235. [CrossRef]
36. Jiang, B.; Liu, J.; Zhang, Y.; Chang, Y.; Wang, Y.; Xue, C. Natural glycosylation modulates the digestive fate of a marine glycoprotein: Insights from sea cucumber major yolk protein. *Food Chem.* **2025**, *492*, 145327. [CrossRef]
37. Honda, A.; Kamada, K.; Seino, J.; Hirayama, H.; Fujihira, H.; Ueki, M.; Shiraki, T.; Burton-Smith, R.N.; Murata, K.; Ishii, N.; et al. Structural characterization of zebrafish Ngly2, an ovary-enriched acid PNGase required for egg-free glycan production. *J. Biol. Chem.* **2025**, *301*, 110906. [CrossRef]
38. Gao, W.; Li, H.; Liu, Y.; Liu, Y.; Feng, X.; Liu, B.F.; Liu, X. Rapid and sensitive analysis of N-glycans by MALDI-MS using permanent charge derivatization and methylamidation. *Talanta* **2016**, *161*, 554–559. [CrossRef]
39. Niu, X.; He, Z.; Li, W.; Wang, X.; Zhi, W.; Liu, F.; Qi, L. Immunomodulatory activity of the glycoprotein isolated from the chinese yam (dioscorea opposita thunb). *Phytother. Res.* **2017**, *31*, 1557–1563. [CrossRef] [PubMed]
40. Sheu, K.M.; Hoffmann, A. Functional hallmarks of healthy macrophage responses: Their regulatory basis and disease relevance. *Annu. Rev. Immunol.* **2022**, *40*, 295–321. [CrossRef] [PubMed]
41. Kohchi, C.; Inagawa, H.; Nishizawa, T.; Soma, G.I. ROS and innate immunity. *Anticancer. Res.* **2009**, *29*, 817–821.
42. Brown, G.C.; Borutaite, V. Interactions between nitric oxide, oxygen, reactive oxygen species and reactive nitrogen species. *Biochem. Soc. Trans.* **2006**, *34*, 953–956. [CrossRef]
43. Guo, Q.; Bi, D.; Wu, M.; Yu, B.; Hu, L.; Liu, C.; Gu, L.; Zhu, H.; Lei, A.; Xu, X. Immune activation of murine RAW264.7 macrophages by sonicated and alkalized paramylon from euglena gracilis. *BMC Microbiol.* **2020**, *20*, 171. [CrossRef] [PubMed]
44. Li, C.; Deng, C.; Wang, S.; Dong, X.; Dai, B.; Guo, W.; Guo, Q.; Feng, Y.; Xu, H.; Song, X. A novel role for the ROS-ATM-Chk2 axis mediated metabolic and cell cycle reprogramming in the M1 macrophage polarization. *Redox Biol.* **2024**, *70*, 103059. [CrossRef]
45. Chen, Y.; Hu, M.; Wang, L.; Chen, W. Macrophage M1/M2 polarization. *Eur. J. Pharmacol.* **2020**, *877*, 173090. [CrossRef]
46. Sica, A.; Mantovani, A. Macrophage plasticity and polarization: In vivo veritas. *J. Clin. Investig.* **2012**, *122*, 787–795. [CrossRef]
47. Li, M.; Wen, J.; Huang, X.; Nie, Q.; Wu, X.; Ma, W.; Nie, S.; Xie, M. Interaction between polysaccharides and toll-like receptor 4: Primary structural role, immune balance perspective, and 3d interaction model hypothesis. *Food Chem.* **2022**, *374*, 131586. [CrossRef] [PubMed]
48. Kim, H.J.; Kim, H.; Lee, J.H.; Hwangbo, C. Toll-like receptor 4 (TLR4): New insight immune and aging. *Immun. Ageing* **2023**, *20*, 67. [CrossRef]
49. Yu, Y.; Zhu, H.; Shen, M.; Yu, Q.; Chen, Y.; Mo, S.; Xie, J. Sulfated cyclocarya paliurus polysaccharides exert immunomodulatory potential on macrophages via Toll-like receptor 4 mediated MAPK/NF-κB signaling pathways. *Food Sci. Hum. Wellness* **2024**, *13*, 115–123. [CrossRef]
50. Zhao, Y.Z.; Wang, Y.L.; Yu, Y. Immunoenhancement effect of cinobufagin on macrophages and the cyclophosphamide-induced immunosuppression mouse model. *Int. Immunopharmacol.* **2024**, *131*, 111885. [CrossRef] [PubMed]
51. Wang, D.; Yang, Y.; Li, J.; Wang, B.; Zhang, A. Enhancing immune responses to inactivated foot-and-mouth virus vaccine by a polysaccharide adjuvant of aqueous extracts from *Artemisia rupestris* L. *J. Vet. Sci.* **2021**, *22*, e30.
52. Ushio-Fukai, M.; Ash, D.; Nagarkoti, S.; Belin de Chantemele, E.J.; Fulton, D.J.R.; Fukai, T. Interplay between reactive oxygen/reactive nitrogen species and metabolism in vascular biology and disease. *Antioxid. Redox Signal.* **2021**, *34*, 1319–1354.
53. Zhang, B.; Lian, W.; Zhao, J. Toll-like receptor 4 and the inflammation during aging. *J. Gerontol. Geriatr.* **2022**, *69*, 471.
54. Bowen, W.S.; Svrivastava, A.K.; Batra, L.; Barsoumian, H.; Shirwan, H. Current challenges for cancer vaccine adjuvant development. *Expert Rev. Vaccines* **2018**, *17*, 207–215. [CrossRef] [PubMed]

Disclaimer/Publisher's Note: The statements, opinions and data contained in all publications are solely those of the individual author(s) and contributor(s) and not of MDPI and/or the editor(s). MDPI and/or the editor(s) disclaim responsibility for any injury to people or property resulting from any ideas, methods, instructions or products referred to in the content.